The Journal of Chemical Physics

# Dynamics of an adenine-adenine RNA conformational switch from discrete path sampling

Cite as: J. Chem. Phys. **150**, 125101 (2019); https://doi.org/10.1063/1.5070152
Submitted: 19 October 2018 . Accepted: 22 February 2019 . Published Online: 29 March 2019

Debayan Chakraborty, and David J. Wales

COLLECTIONS

Paper published as part of the special topic on Markov Models of Molecular Kinetics
Note: This article is part of the Special Topic "Markov Models of Molecular Kinetics" in J. Chem. Phys.

View Online Export Citation CrossMark

ARTICLES YOU MAY BE INTERESTED IN

The mechanism of RNA base fraying: Molecular dynamics simulations analyzed with core-set Markov state models
The Journal of Chemical Physics **150**, 154123 (2019); https://doi.org/10.1063/1.5083227

Committors, first-passage times, fluxes, Markov states, milestones, and all that
The Journal of Chemical Physics **150**, 054106 (2019); https://doi.org/10.1063/1.5079742

On the removal of initial state bias from simulation data
The Journal of Chemical Physics **150**, 104105 (2019); https://doi.org/10.1063/1.5063556




© 2019 Author(s).

AIP Publishing

The Journal of Chemical Physics ARTICLE scitation.org/journal/jcp

# Dynamics of an adenine-adenine RNA conformational switch from discrete path sampling

Cite as: J. Chem. Phys. 150, 125101 (2019); doi: 10.1063/1.5070152
Submitted: 19 October 2018 • Accepted: 22 February 2019 •
Published Online: 29 March 2019

View Online Export Citation CrossMark

Debayan Chakraborty[1,a] and David J. Wales[2,b]

## AFFILIATIONS

[1] Department of Chemistry, The University of Texas at Austin, Austin, Texas 78712, USA
[2] Department of Chemistry, University of Cambridge, Lensfield Road, Cambridge CB2 1EW, United Kingdom

**Note:** This article is part of the Special Topic "Markov Models of Molecular Kinetics" in J. Chem. Phys.
[a] **Electronic mail:** debayan.chakraborty@utexas.edu
[b] **Electronic mail:** dw34@cam.ac.uk

## ABSTRACT

The study of "rare event" dynamics can be challenging despite continuing advances in computer hardware. A wide variety of methods based on the master equation approach have been developed to tackle such problems, where the focus is on Markovian dynamics between appropriately defined states. In this contribution, we employ the discrete path sampling approach to characterize pathways and rates for an adenine-adenine RNA conformational switch. The underlying free energy landscape supports competing structures separated by relatively high barriers, with the two principal funnels leading to the major and minor conformations identified by NMR experiments. The interconversion time scale is predicted to be a few hundred seconds, consistent with the experimental lower bound estimates. We find that conformational switching occurs via stacked intermediates, through a sliding mechanism, in agreement with a previous simulation study. By retaining full dimensionality and avoiding low-dimensional projections, the mechanism can be described at an atomistic level of detail.

*Published under license by AIP Publishing.* https://doi.org/10.1063/1.5070152

## I. INTRODUCTION

Structural plasticity plays a key role in endowing RNA with unique capabilities and is critical to its function, both as a catalyst and a binding partner.[1,2] Conformational transitions in RNA occur over a hierarchy of time scales[2] and are often associated with long waiting times, corresponding to kinetic trapping in metastable states.[3–5] The manifestation of such rare event dynamics makes it difficult to obtain detailed insight into conformational transitions of biological relevance using conventional simulation techniques.

A considerable effort has been directed towards advancing enhanced sampling methods, many of which are now quite routinely used in unravelling various facets of RNA dynamics and thermodynamics. For example, different implementations of replica-exchange molecular dynamics (REMD) and parallel tempering,[6–8] as well as metadynamics,[9,10] have been used to explore the free energy landscapes of prototypical RNA hairpins and hence suggest possible folding pathways. Applications of these thermodynamic sampling techniques to more complex RNA molecules are also emerging.[11,12] However, extracting meaningful kinetic information is not straightforward for these methods, although various recipes for recovering dynamical information have been suggested.[13,14]

Alternative efforts focused upon dynamics have employed the master equation framework[15,16] to construct kinetic transition networks.[17–19] This approach has a long history in the context of chemical kinetics and was probably first applied to relaxation dynamics in atomic clusters by Kunz and co-workers.[20–23] There have now been numerous applications to dynamical transitions in proteins, and more recently to RNA folding and conformational switching.[24,25] Two distinct approaches have been employed to construct the corresponding networks. Methods based on geometry optimization characterize stationary points of the potential energy surface, namely, local minima and the transition states that connect them via steepest-descent paths, with post-processing using the tools of statistical mechanics and unimolecular rate theory.[19,26,27] Alternatively, if the conformations of interest can be


Published under license by AIP Publishing

connected using explicit dynamics, then a network can be constructed by defining suitable states and their interconversion rates; this approach is often called Markov state modeling.[28–35] A variety of rare event methods based upon explicit dynamics have now been developed that focus on enhanced sampling in some form.[36–48] The geometry optimization and explicit dynamics methodologies are quite complementary: geometry optimization schemes do not suffer from trapping due to high barriers and slow time scales, but entail additional approximations in extracting observable properties.

In the present contribution, we focus on networks constructed from geometry optimization, which exploit a coarse-grained description of the underlying landscape in terms of stationary points, where transition pathways between different metastable conformations are defined by "discrete paths," consisting of interconnected minima and transition states (saddle points of index one[49]). The discrete path sampling (DPS) technique[50,51] is used to systematically sample such discrete paths between states of interest to construct a transition network, which encodes the thermodynamic as well as kinetic information. In our recent studies on nucleic acid dynamics,[52–57] we have used DPS to reproduce and explain experimental results from the viewpoint of energy landscape theory, providing atomistic level insight into the pathways underlying key conformational transitions.

We employ the DPS technique to characterize the conformational switching pathways for a non-canonical adenine-adenine (AA) base pair[58] located at the centre of a nine base pair RNA duplex (Fig. 1). Experiments by Turner and co-workers[59] indicate that the two adenines can exchange positions and switch between major and minor forms, which differ only in the base-stacking pattern along the minor groove. Based on NMR chemical shifts, the authors estimated a lower bound for the exchange rate of 300 $s^{-1}$. In a subsequent study,[60] Mathews and co-workers employed targeted molecular dynamics (TMD), as well as the nudged elastic band (NEB)[61,62] method, to map out pathways between the major and the minor conformations. Their results suggested that the conformational switch preferentially occurs via intermediates where the two adenines are stacked, rather than hydrogen-bonded. Surprisingly, various combinations of force fields and simulation strategies predicted the minor form to be thermodynamically more stable compared to the major form, which seems inconsistent with experiments.

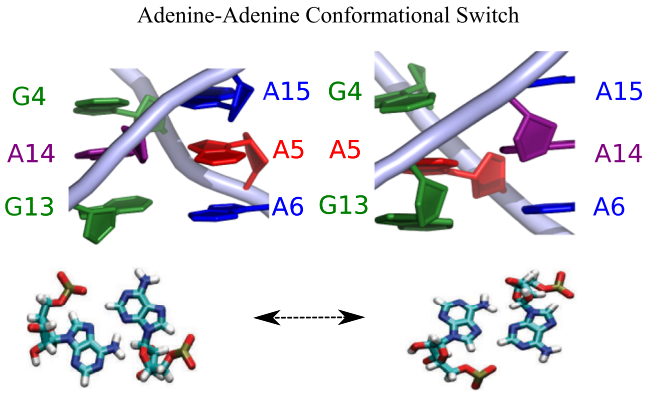


**FIG. 1**. The RNA duplex considered in this study. In the minor form (shown on the left), A5 is stacked between A6 and A15. In the major form (shown on the right), A14 is stacked between A6 and A15. In both duplex conformations, the central adenine-adenine base pair exhibits a trans-Hoogsteen/sugar-edge hydrogen-bonding pattern.

Our results indicate that the major and minor forms predicted by the NMR experiments lie at the bottom of two principal funnels on the energy landscape. The most kinetically relevant transition pathway between the two conformations features stacked intermediates, in agreement with Mathews and co-workers.[60] Our calculated conformational switching rate from the minor to the major form is 166 $s^{-1}$, in quantitative agreement with the experimental lower bound estimate.[60] Furthermore, we obtain the correct ordering of free energies for the major and the minor form. It is possible that force field inaccuracies, or problems caused by the projections associated with low-dimensional reaction coordinates, may have resulted in a reversal of thermodynamic stabilities in the earlier study.

## II. METHODOLOGY

### A. System setup

The initial coordinates for the major and minor forms of the RNA duplex were taken from structures deposited in the protein data bank (PDB) database (PDB ID: 2DD2 and 2DD3, respectively).[59] Following Mathews and co-workers,[60] we truncated the system by removing the dangling ends consisting of unpaired uracil and purine. The RNA molecule was modeled using a properly symmetrized version[63] of the AMBER99bsc0 force field,[64] employing the $\chi$OL3 torsional corrections.[65] Solvent effects were treated implicitly using a generalized Born model.[66,67]

In their experimental study, Turner and co-workers carried out NMR experiments[59] at two different effective salt concentrations (80 mM and 1M NaCl). The NMR spectra recorded at the two salt concentrations were analogous, with the major and the minor form exhibiting a similar pattern of nuclear Overhauser effects (NOEs). Mathews and co-workers,[59] in their simulation study, employed a salt concentration of 1M to explore the dynamical features of the conformational switch over short time scales, map out the free energy profile using umbrella sampling, and estimate the free energy difference between the two NMR conformations. Here, we use an effective salt concentration of 1M using the Debye-Hückel approximation[68] with the intention to directly compare our results to the NMR experiments, as well as the previous simulations.

### B. Molecular dynamics simulations

The graphics processor unit (GPU) enabled version of the AMBER12 code was used to carry out implicit solvent molecular dynamics simulations of length 50 ns starting from local potential energy minima corresponding to the major and minor forms. No cutoffs were employed for the non-bonded interactions. The simulation temperature was maintained at 300 K using a Langevin thermostat.[69]

### C. Discrete path sampling

DPS simulations were carried out to survey the underlying energy landscape and characterize the transition pathways for the adenine-adenine conformational switch in full dimensionality.


Published under license by AIP Publishing

The DPS procedure provides a systematic framework based on geometry optimization for building a kinetic transition network, which encodes the global thermodynamics and kinetics.[50,51,70] A sequence of minima connected by intervening transition states constitutes a discrete path. A local minimum is defined as a stationary point (vanishing gradient) for which all the nonzero normal mode frequencies are positive. Transition states are defined geometrically as saddle points of index one,[49] with a single imaginary normal mode frequency corresponding to a local reaction coordinate. Steepest-descent paths from the transition state define the connected local minima. Here, we employed a modified version of the limited memory Broyden-Fletcher-Goldfarb-Shanno (L-BFGS) algorithm[71] for local minimizations to characterize approximate steepest-descent paths. The doubly-nudged[72] elastic band[61,62] (DNEB) method was used to find candidate transition state structures between intervening minima. These transition state candidates were further optimized using hybrid-eigenvector-following.[73,74] We note that it is important to establish the connectivity of local minima by checking the steepest-descent pathways since the original DNEB interpolation often misses some of the intervening transition states and local minima, especially for lengthy gaps when a small number of images are used. It is also noteworthy that the kinetic transition network usually requires substantial additional sampling to identify kinetically relevant pathways once an initial connected path has been found.

A convergence criterion of $10^{-6}$ kcal/(mol A) for the root-mean-square gradient was employed for all the geometry optimizations. The OPTIM code[75] interfaced with the AMBER9 package[76] was used to carry out the local minimizations, the transition state searches, and pathway analysis.

Representative structures corresponding to the major and minor conformations identified from the MD simulations were used as the initial endpoints for the DPS calculations. After a fully connected initial discrete path was found between the two structures, further refinement of the resulting kinetic transition network was carried out using several schemes available within the PATHSAMPLE code.[77] These schemes have been described in detail elsewhere, and for brevity, we will only outline the key features. To locate pathways with lower energy barriers, we used the SHORTCUT BARRIER scheme,[78–80] which selects pairs of minima on either side of, and an equal number of steps away from, the largest barriers for additional connection attempts. The SHORTCUT scheme,[78–80] which attempts to connect minima that are close together in configuration space, but are separated by a minimum number of steps on the discrete paths, was used to locate shorter paths between the endpoints. Finally, the UNTRAP scheme,[79] which selects minima for connection-making attempts based on the ratio of the potential energy barrier to the potential energy difference, was used to remove artificial frustration from the transition network, which provides a more faithful representation of the global dynamics. The three refinement schemes were used in sequence until the rate constant for the transition between the major and minor forms was converged to within an order of magnitude. Given the systematic sources of error in the empirical potential, the sampling, the use of harmonic densities of states, and the assumption of Markovian dynamics between appropriately regrouped states,[81] we would not expect better than order of magnitude agreement with experiments. Further details regarding the evaluation of the free energies and rate constants are included in the Appendix.

### D. Disconnectivity graphs

The potential and free energy landscapes constructed using DPS were visualized in the form of disconnectivity graphs.[82–84] In these diagrams, the landscape is segregated into disjoint sets of minima known as superbasins, at regular intervals of energy. Minima within each superbasin are mutually accessible via transition states lying below the energy threshold, while transitions out of superbasins require higher energy barriers to be surmounted. A key feature of disconnectivity graphs is that they should provide a faithful representation of the landscape,[85] avoiding low-dimensional projection, which may lump together states separated by significant energy barriers.

## III. RESULTS AND DISCUSSION

Although the time scale of the MD simulations is not long enough to explore complete conformational switching between the major and minor forms, they provide some useful insight into the local fluctuations around the NMR structures. As illustrated by the time evolution of the root mean square deviation (RMSD) (Fig. 2), the minor conformation is quite flexible, whereas the major conformation seems to exhibit some degree of conformational rigidity over short time scales. The large jumps in the RMSD profile for both the major and minor forms are associated with flipping of the A5 nucleobase out of the helix, which in turn leads to the loss of the hydrogen-bonding interactions between the central adenine-adenine sheared base pair.

In contrast to short time scale MD simulations, discrete path sampling provides a viable route to global exploration of the underlying energy landscape and facilitates the detailed study of transition pathways of varying complexity. To identify suitable endpoints for DPS simulations, snapshots along the MD trajectories were saved every 10 ps and subsequently locally minimized. The

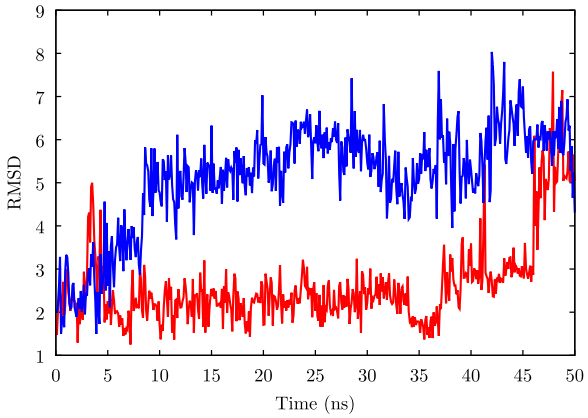


**FIG. 2.** Evolution of the RMSD for the major conformation (red) and the minor conformation (blue) along the MD trajectories. The large jumps in the profiles correspond to the flipping of the A5 nucleobase into an extrahelical position.


Published under license by AIP Publishing

lowest potential energy minima corresponding to the minor and major forms were selected as the representative reactant and product states, respectively. After an initial discrete pathway was found between these endpoints, connection attempts were made for the rest of the local minima (identified from the MD simulations) to either the reactant or the product state in a pairwise fashion, based on the shortest distance in configuration space after optimal alignment. The transition network was subsequently refined employing the strategies described in Sec. II.

The free energy landscape for the RNA duplex, computed at 300 K, is shown in the form of a disconnectivity graph in Fig. 3. To highlight the key regions of the landscape, we have used a discrete coloring scheme. The red branches denote minima that exhibit an RMSD ≤1 Å from the NMR structure corresponding to the major form. Similarly, the blue branches denote minima that are close to the NMR structure corresponding to the minor form. All the other branches are colored black. The intermingling of colors in some regions of the landscape emphasizes that simple structural order parameters, such as RMSD, do not distinguish kinetically separate basins. We note that the use of structural metrics in this study is only to aid visualization, not to calculate kinetic properties.

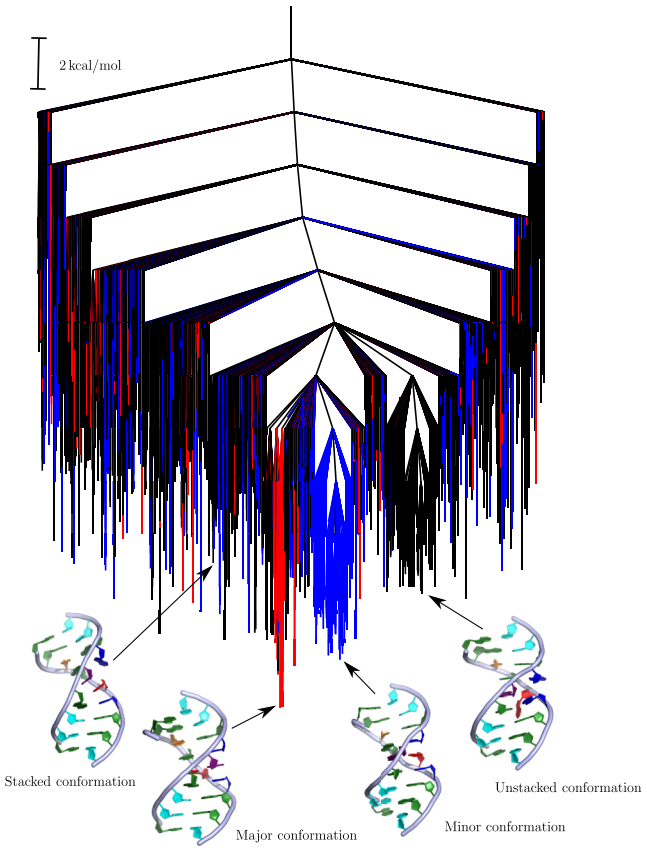


**FIG. 3**. Free energy landscape computed at 300 K depicted in the form of a disconnectivity graph. The red branches lead to minima that exhibit an RMSD ≤1 Å from the NMR structure corresponding to the major conformation (PDB ID: 2DD2). Similarly, blue branches lead to minima that exhibit an RMSD ≤1 Å from the NMR structure corresponding to the minor conformation (PDB ID: 2DD3). All other branches are shown in black. Some representative minima from the different structural ensembles are shown superimposed on the graph.

As expected, the putative free energy global minimum corresponds to the major conformation. The lowest energy conformation lying at the bottom of the red funnel exhibits all the key interactions found in the NMR structure: A14 is stacked between A6 and A15 along the minor groove and the A5-A14 base pair exhibits trans-Hoogsteen/sugar-edge hydrogen-bonding interactions. In contrast, A5 is stacked between A6 and A15 in the minor conformation, which lies at the bottom of the blue funnel. The minor form is destabilized by about 1.8 kcal/mol with respect to the major form. This estimate is in good agreement with the upper bound of the experimental free energy difference (around 1.3 kcal/mol), calculated based on the population analysis of the major and the minor form. However, our results differ from the earlier study by Mathews and co-workers,[59] who predicted that the minor form is stabilized by around 7.04 kcal/mol. In that work, the authors estimated the free energy difference based on a one-dimensional representation of the free energy surface along a predefined reaction coordinate. It is possible that the low-dimensional projection could have resulted in the opposite stability that was reported.

In addition to the major and the minor form, we also identify another prominent funnel on the landscape, which primarily consists of structures in which the A5 nucleobase is flipped out of the RNA helix. In fact, these structures are quite similar to those that were encountered during the initial MD simulations. The stacked conformation, which was predicted by Mathews and co-workers to be a key intermediate along the conformational switching pathway,[60] lies at the bottom of a narrow subfunnel.

The overall topography of the landscape leads to multiple peaks in the heat capacity profile (Fig. 4). Such features are characteristic of multifunnel landscapes associated with conformational switches[54,86,87] and were first observed for the solid-solid type transition between competing morphologies observed in atomic clusters.[88,89] At low temperatures, where enthalpy dominates, the major conformation is thermodynamically favored, although kinetic trapping in the competing basins is likely to impede relaxation. At intermediate temperatures, the competing effects of enthalpy and

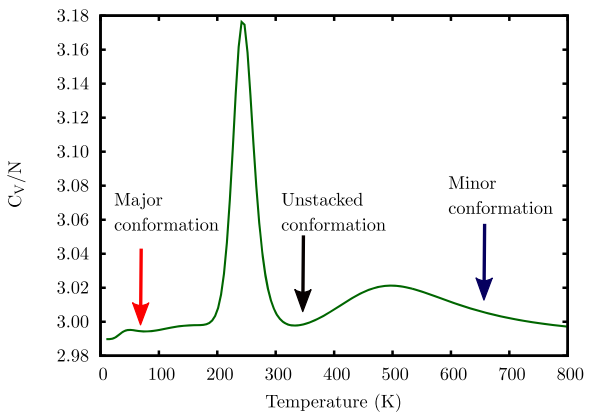


**FIG. 4**. Heat capacity profile obtained from the database of minima using the harmonic superposition approximation. Here, $C_V$ is in reduced units of $k$, and scaled by $N$.


Published under license by AIP Publishing

entropy cause the free energy global minimum to switch to the unstacked conformation. At high temperatures, the minor conformation dominates the equilibrium population. It is likely that the transition temperatures associated with the switching between the different funnels may be overestimated here due to the inherent limitations of the harmonic superposition approximation.[70] Nonetheless, the relative positions of the peaks in the heat capacity curve provide additional insight into the contrasting flexibilities of the major and the minor form observed during the MD simulations. The major conformation, which is stabilized by enthalpy, undergoes only restricted motions for much of the trajectory. On the other hand, the minor form is more flexible and exhibits substantially larger fluctuations.

The large free energy barrier separating the major and the minor conformation suggests that conformational switching between the two forms is a slow process. Using the new graph transformation (NGT) technique[90,91] in conjunction with a regrouping threshold of 5.0 kcal/mol, we estimate a rate constant of 166 $s^{-1}$ for the transition from the minor to the major form and 247 $s^{-1}$ for the reverse process, which is in good agreement with experiments.[59] A representative sequence of configurations from the corresponding pathway ensemble is shown in Fig. 5. The initial phase of the transition is characterized by the disruption of the hydrogen-bonds between the sheared adenine-adenine base pair. During this phase, A5 loses its stacking interactions with both A6 and A15. Subsequently, the stacked intermediate structure is formed, where A14 is stacked on top of A5. During the next phase, A14 continues to slide towards the minor groove, until the hydrogen-bonding interaction between A5 and A14 is reestablished, and the major conformation is formed.

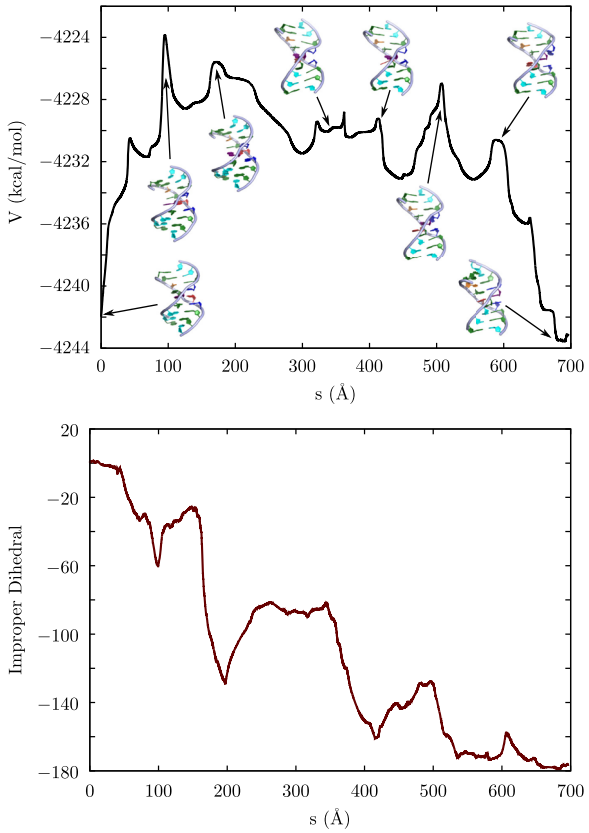


**FIG. 5**. Top panel: total potential energy ($V$) as a function of the integrated path length ($s$) for the conformational switch from the minor to the major form. This pathway makes the largest contribution to the phenomenological two-state rate constant and hence is assigned as the kinetically most relevant. Some representative structures encountered along the pathway are illustrated. Bottom panel: the evolution of the improper dihedral defined by the C4, C8, and N1 atoms of A5 and the C5 atom of A14, along the pathway.

In a previous study, an improper dihedral angle defined by the C4, C8, and N1 atoms of A5 and the C5 atom of A14 was employed as a surrogate for the multidimensional reaction coordinate corresponding to the sliding mechanism.[60] We find that the value of this dihedral gradually changes from around 0° to −180° along the transition pathway, in a similar fashion to the 5′ facing mechanism.[60] However, the dihedral profile features jumps and exhibits plateaux, in contrast to the relatively smooth profile reported before. This discrepancy suggests that there are additional degrees of freedom coupled to the dihedral coordinate, which could have important implications in the analysis of thermodynamics and kinetics. Stationary points in which the improper dihedral exhibits values in the range from 0° to 180° are also present in our transition network. However, the corresponding transition states are connected to the adjoining minima via high energy barriers. Therefore, 3′ facing pathways are associated with relatively low statistical weights in the overall description of the rate constant and are unlikely to be major contributors to the global dynamics. These paths are likely to be associated with more flux and compete with the 5′ facing mechanism as the temperature is increased. Our results are in accord with previous simulations by Mathews and co-workers,[60] which predicted the 5′ facing pathway to be more favorable and identified the 3′ mechanism only when additional restraints were employed.

## IV. CONCLUSION

In this study, we have provided atomistic insight into the transition mechanism between two conformations of an adenine-adenine RNA conformational switch using discrete path sampling. The interconversion kinetics are relatively slow, making this a challenging problem for conventional simulation techniques. Conformational switching between the two forms occurs via stacked intermediates, along a preferred sliding direction. Overall, the generic features of the transition pathway are found to be consistent with a previous study by Mathews and co-workers.[59]

In agreement with the experimental findings,[59] we find that the major form is stabilized by around 1.8 kcal/mol with respect to the minor form in terms of free energy. The interplay between enthalpy and entropy leads to multiple features in the heat capacity profile. Such signatures are likely to be characteristic of conformational switches and suggest that a subtle modulation of environmental conditions could result in population shifts to favor one particular form. In the future, it would be interesting to see how the landscape evolves as a function of tunable parameters, which could provide further insight into the remarkable functionality of more complex conformational switches.


Published under license by AIP Publishing

Current RNA force fields are far from perfect and can have a significant impact on the outcome of simulations. There have been continued efforts to refine RNA force field parameters and to obtain a more faithful description of structure and energetics.[7,92–97] As outlined in a recent review by Šponer and co-workers,[98] the AMBER99bsc0 force field in conjunction with the $\chi$OL3 correction, which was employed in this study, is currently preferred for describing the structure and dynamics of RNA at the all-atom level. Various reparametrization schemes for the other torsion angles,[92] as well as non-bonded interactions,[7] have also been suggested, but their behavior may not be optimal for A-RNA simulations. In conjunction with various enhanced sampling techniques, such as replica exchange molecular dynamics[8] and metadynamics,[9] the AMBER99bsc0$\chi$OL3 force field has been successfully used to yield microscopic insight into various aspects of RNA folding. In a recent study, Case and co-workers demonstrated that several NMR observables, including NOEs and residual dipolar couplings (RDCs) for a prototypical RNA hairpin, can be accurately reproduced with the AMBER99bsc0$\chi$OL3 force field.[99] Nearly all studies to date employing this force field use an explicit description of the solvent environment and the counterion atmosphere. In particular, the inclusion of monovalent and divalent ions, such as $Na^+$ and $Mg^{2+}$, becomes critical in simulations of RNA self-assembly into higher order structures, where counterion condensation and stabilization of tertiary interactions via specific ion binding are important factors.[100] However, the use of an implicit solvent model is desirable within the potential energy landscape simulation framework because the inclusion of solvent molecules and counterions would lead to rather noisy landscapes, with stationary points corresponding to minor rearrangements in the solvent structure or ion distribution. This unwanted noise would make it harder to extract transition pathways and draw key mechanistic insight.

Although an implicit description of the surrounding solvent and counterions reduces the number of stationary points, based on our earlier work on small nucleic acids,[52–54] we believe that the implicit solvent landscape should capture the essential features of the underlying physics. For example, using the AMBER99bsc0$\chi$OL3 force field in conjunction with the generalized Born solvent model, we could accurately reproduce the experimental rate constants and relative ordering of free energy minima for prototypical UUCG and GCAA tetraloop hairpins.[52] Similarly, an implicit solvent description seems sufficient for the adenine-adenine conformational switch, as the emergent thermodynamic and kinetic properties are in accord with experiments. If an explicit description of solvent molecules and counterions is employed, we do expect some systematic shift in the heat capacity profile, as well as rate constant estimates, and perhaps some reordering of minima within the major free energy basins, but we believe that our principal conclusions would not change substantially. In a future study, it would be interesting to investigate these aspects systematically.

## ACKNOWLEDGMENTS

This research was funded by the EPSRC and the ERC. D.C. would like to thank the Cambridge Commonwealth, European, and International Trusts for providing a scholarship while he was a Ph.D. student at the University of Cambridge.

## APPENDIX: ESTIMATING FREE ENERGIES AND INTERCONVERSION RATES

The vibrational partition functions associated with the minima and the transition states in the network were estimated using a harmonic approximation[101,102]

$$Z_i(T) = \frac{n_i e^{-V_i/kT}}{(h\bar{\nu}_i/kT)^{\kappa}}. \tag{A1}$$

In Eq. (A1), $V_i$ denotes the potential energy of minimum $i$, $n_i$ is the number of distinct permutational isomers of $i$, $\bar{\nu}_i$ denotes the geometric mean normal mode frequency associated with minimum $i$, and $\kappa = 3N - 6$ is the number of vibrational degrees of freedom, where $N$ is the number of atoms.

The full canonical partition function, $Z(T)$, can be written as a sum of all the contributions from the different catchment basins corresponding to each local minimum

$$Z(T) = \sum_i^N Z_i(T). \tag{A2}$$

The local free energy, $F_i(T)$, and the equilibrium occupation probability, $p_i^{eq}(T)$, of each minimum are

$$F_i(T) = -kT \ln Z_i(T), \tag{A3}$$

and

$$p_i^{eq}(T) = \frac{Z_i(T)}{Z(T)}. \tag{A4}$$

The partition functions and the free energies for the transition states are defined in an analogous way, except that the normal mode frequency corresponding to the unique negative Hessian eigenvalue (imaginary normal mode frequency) is excluded.

The minimum-to-minimum rate constants are estimated using harmonic transition state theory (TST)

$$k_i^{\dagger}(T) = \frac{kT}{h}\frac{Z^{\dagger}(T)}{Z_i(T)} e^{-\beta \Delta V}. \tag{A5}$$

In Eq. (A5), $Z^{\dagger}(T)$ denotes the partition function of the transition state, $Z_i(T)$ is the partition function of minimum $i$, and $\Delta V$ is the potential energy difference between the transition state and minimum $i$. The total rate constant $k_{ji}(T)$ for an elementary transition from minimum $i$ to minimum $j$ is obtained by summing the $k_i^{\dagger}(T)$ values for all transition states that connect the two minima.

The minimum-to-minimum rate constants are used in calculating global dynamical properties. Within the steady-state approximation for intervening minima, the rate constants, $k_{AB}^{SS}$ and $k_{BA}^{SS}$ between reactant (A) and product (B) states, can be expressed as weighted sums over all discrete paths in the network, assuming that the dynamics between adjacent minima or lumped states[81] are Markovian[50]

$$k_{AB}^{SS} = \frac{1}{p_B^{eq}} \sum_{a \leftarrow b} \frac{k_{ai_1} k_{i_1 i_2} k_{i_2 i_3} \ldots k_{i_n b} p_b^{eq}}{\sum_{j_1} k_{j_1 i_1} \sum_{j_2} k_{j_2 i_2} \sum_{j_3} k_{j_3 i_3} \ldots \sum_{j_n} k_{j_n i_n}}. \tag{A6}$$

In terms of transition probabilities, $P_{\gamma\alpha}$ between directly connected minima $\gamma$ and $\alpha$, Eq. (A6) can be rewritten as[50]


Published under license by AIP Publishing

$$k_{AB}^{SS} = \frac{1}{p_B^{eq}} \sum_{a \leftarrow b} P_{ai_1} P_{i_1 i_2} P_{i_2 i_3} \ldots P_{i_n b} p_b^{eq} \tau_b^{-1}. \quad \text{(A7)}$$

The individual sums in the denominators of Eq. (A6) consist of the unimolecular rate constants for all direct transitions from minimum $j_k$ to $i_k$. The discrete path that makes the largest contribution to the steady-state rate constant is termed the "fastest path" and can be extracted from the network using Dijkstra's shortest path algorithm with appropriate edge weights[78,103] $-\ln P_{\alpha\beta}$, providing access to the product of transition probabilities in Eq. (A7). To characterize additional paths in the order of their contribution to $k^{SS}$, we employ the recursive enumeration algorithm[104] within the same framework,[105] and these pathways were examined to deduce mechanistic details of the adenine-adenine conformational switch. The steady-state approximation for the intervening minima can be relaxed to yield rate constants $k_{AB}$ and $k_{BA}$ that correspond to the mean first passage times (MFPTs) between reactants and products.[90] To extract these values, we employ a graph transformation technique (NGT)[90,106] where minima in the intervening region are progressively removed, and the transition probabilities as well as the waiting times are renormalised to conserve the average mean first passage time (MFPT).[90,91]

We compute the rate constants in conjunction with a recursive free energy regrouping scheme,[81] which lumps together structures separated by free energy barriers below a certain threshold into a single macrostate. This approach is similar in spirit to the kinetic clustering schemes employed in methods based upon explicit dynamics.[26,33] In the regrouping, the original reactant and product states are expanded into ensembles of conformations assumed to be in local equilibrium, and hence, the global dynamics can be directly compared to the observation time scale of experiments.[107] After regrouping, the equilibrium occupation probability and the free energy associated with group $J$ are

$$p_J^{eq}(T) = \sum_{j \in J} p_j^{eq}(T), \quad \text{(A8)}$$

$$F_J = -kT \ln \sum_{j \in J} Z_j(T), \quad \text{(A9)}$$

where minimum $j$ is a member of group $J$. The free energy of the group of transition states linking $J$ and $K$ is[81]

$$F_{KJ}^{\dagger} = -kT \ln \sum_{k \leftarrow j} Z_{kj}^{\dagger}(T) \equiv -kT \ln Z_{KJ}^{\dagger}(T). \quad \text{(A10)}$$

To analyze global dynamics corresponding to regrouped databases, the rate constants corresponding to transitions between different free energy groups are required, which can then be used in the appropriate expressions for rate constants and committor probabilities.[90] The intergroup rate constant from $J$ to $K$ is[81]

$$k_{KJ} = \sum_{k \leftarrow j} \frac{p_j^{eq}(T)}{p_J^{eq}(T)} k_{kj}(T) = \sum_{k \leftarrow j} \frac{Z_j(T)}{Z_J(T)} \frac{kT}{h} \frac{Z_{kj}^{\dagger}(T)}{Z_j(T)}$$
$$= \frac{kT}{h} \frac{Z_{KJ}^{\dagger}(T)}{Z_J(T)} = \frac{kT}{h} e^{-\left[F_{KJ}^{\dagger}(T) - F_J(T)\right]/kT}. \quad \text{(A11)}$$

## REFERENCES


[1] A. M. Mustoe, C. L. Brooks, and H. M. Al-Hashimi, "Hierarchy of RNA functional dynamics," Annu. Rev. Biochem. **83**(1), 441–466 (2014).
[2] E. A. Dethoff, J. Chugh, A. M. Mustoe, and H. M. Al-Hashimi, "Functional complexity and regulation through RNA dynamics," Nature **482**, 323–330 (2012).
[3] D. Thirumalai and S. A. Woodson, "Kinetics of folding of proteins and RNA," Acc. Chem. Res. **29**(9), 433–439 (1996).
[4] D. Thirumalai and C. Hyeon, "RNA and protein folding: Common themes and variations," Biochemistry **44**, 4957–4970 (2005).
[5] J. Chin Lin, C. Hyeon, and D. Thirumalai, "RNA under tension: Folding landscapes, kinetic partitioning mechanism, and molecular tensegrity," J. Phys. Chem. Lett. **3**(23), 3616–3625 (2012).
[6] A. E. Garcia and D. Paschek, "Simulation of the pressure and temperature folding/unfolding equilibrium of a small RNA hairpin," J. Am. Chem. Soc. **130**(3), 815–817 (2008).
[7] A. A. Chen and A. E. Garcia, "High-resolution reversible folding of hyperstable RNA tetraloops using molecular dynamics simulations," Proc. Natl. Acad. Sci. U. S. A. **110**, 16820–16825 (2013).
[8] P. Kührová, P. Banáš, R. B. Best, J. Šponer, and M. Otyepka, "Computer folding of RNA tetraloops? Are we there yet?," J. Chem. Theory Comput. **9**(4), 2115–2125 (2013).
[9] S. Haldar, P. Kührová, P. Banáš, V. Spiwok, J. Šponer, P. Hobza, and M. Otyepka, "Insights into stability and folding of GNRA and UNCG tetraloops revealed by microsecond molecular dynamics and well-tempered metadynamics," J. Chem. Theory Comput. **11**(8), 3866–3877 (2015).
[10] S. Bottaro, P. Banáš, J. Šponer, and G. Bussi, "Free energy landscape of GAGA and UUCG RNA tetraloops," J. Phys. Chem. Lett. **7**, 4032–4038 (2016).
[11] X. Xue, W. Yongjun, and L. Zhihong, "Folding of SAM-II riboswitch explored by replica-exchange molecular dynamics simulation," J. Theor. Biol. **365**, 265–269 (2015).
[12] Y. Bian, J. Zhang, J. Wang, J. Wang, and W. Wang, "Free energy landscape and multiple folding pathways of an h-type RNA pseudoknot," PLoS One **10**, e0129089 (2015).
[13] N. V. Buchete and G. Hummer, "Peptide folding kinetics from replica exchange molecular dynamics," Phys. Rev. E **77**, 030902 (2008).
[14] P. Tiwary and M. Parrinello, "From metadynamics to dynamics," Phys. Rev. Lett. **111**, 230602 (2013).
[15] N. G. van Kampen, *Stochastic Processes in Physics and Chemistry* (North-Holland, Amsterdam, 1981).
[16] R. E. Kunz, *Dynamics of First-Order Phase Transitions* (Deutsch, Thun, 1995).
[17] F. Noé and S. Fischer, "Transition networks for modeling the kinetics of conformational change in macromolecules," Curr. Opin. Struct. Biol. **18**, 154–162 (2008).
[18] D. Prada-Gracia, J. Gómez-Gardenes, P. Echenique, and F. Fernando, "Exploring the free energy landscape: From dynamics to networks and back," PLoS Comput. Biol. **5**, e1000415 (2009).
[19] D. J. Wales, "Energy landscapes: Some new horizons," Curr. Opin. Struct. Biol. **20**, 3–10 (2010).
[20] R. S. Berry and R. Breitengraser-Kunz, "Topography and dynamics of multidimensional interatomic potential surfaces," Phys. Rev. Lett. **74**, 3951 (1995).
[21] R. E. Kunz and R. S. Berry, J. Chem. Phys. **103**, 1904 (1995).
[22] B. Kunz, R. S. Berry, and T. Astakhova, "Using clusters to relate topography and dynamics of multidimensional potentials," Surf. Rev. Lett. **3**, 307–312 (1996).
[23] R. E. Kunz, P. Blaudeck, K. H. Hoffmann, and R. S. Berry, "Atomic clusters and nanoscale particles: From coarse-grained dynamics to optimized annealing schedules," J. Chem. Phys. **108**, 2576 (1998).
[24] G. Pinamonti, J. Zhao, D. E. Condon, F. Paul, F. Noé, D. H. Turner, and G. Bussi, "Predicting the kinetics of RNA oligonucleotides using Markov state models," J. Chem. Theory Comput. **13**, 926–934 (2017).
[25] B. M. Warfield and P. C. Andersen, "Molecular simulations and Markov state modeling reveal the structural diversity and dynamics of a theophylline-binding RNA aptamer in its unbound state," PLoS One **12**, e0176229 (2017).
[26] D. J. Wales, "Decoding the energy landscape: Extracting structure, dynamics and thermodynamics," Phil. Trans. Roy. Soc. A **370**, 2877–2899 (2012).



Published under license by AIP Publishing

[27]J. A. Joseph, K. Rder, D. Chakraborty, R. G. Mantell, and D. J. Wales, "Exploring biomolecular energy landscapes," Chem. Commun. **53**, 6974–6988 (2017).
[28]C. Schütte, A. Fischer, W. Huisinga, and P. Deuflhard, "A direct approach to conformational dynamics based on hybrid Monte Carlo," J. Comput. Phys. **151**(1), 146–168 (1999).
[29]M. Shirts and V. S. Pande, "Screen savers of the world unite!," Science **290**(5498), 1903–1904 (2000).
[30]N. Singhal, C. D. Snow, and V. S. Pande, "Using path sampling to build better Markovian state models: Predicting the folding rate and mechanism of a tryptophan zipper beta hairpin," J. Chem. Phys. **121**, 415–425 (2004).
[31]W. C. Swope, J. W. Pitera, and F. Suits, "Describing protein folding kinetics by molecular dynamics simulations. I. Theory," J. Phys. Chem. B **108**, 6571–6581 (2004).
[32]J. D. Chodera, K. A. Dill, N. Singhal, V. S. Pande, W. C. Swope, and J. W. Pitera, "Automatic discovery of metastable states for the construction of Markov models of macromolecular conformational dynamics," J. Chem. Phys. **126**, 155101 (2007).
[33]V. S. Pande, K. Beauchamp, and G. R. Bowman, "Everything you wanted to know about Markov state models but were afraid to ask," Methods **52**, 99–105 (2010).
[34]J. H. Prinz, H. Wu, M. Sarich, B. Keller, M. Senne, M. Held, J. D. Chodera, C. Schutte, and F. Nóe, "Markov models of molecular kinetics: Generation and validation," J. Chem. Phys. **134**, 174105 (2011).
[35]B. E. Husic and V. S. Pande, "Markov state models: From an art to a science," J. Am. Chem. Soc. **140**(7), 2386–2396 (2018).
[36]G. A. Huber and S. Kim, "Weighted-ensemble Brownian dynamics simulations for protein association reactions," Biophys. J. **70**, 97–110 (1996).
[37]C. Dellago, P. G. Bolhuis, F. S. Csajka, and D. Chandler, "Transition path sampling and the calculation of rate constants," J. Chem. Phys. **108**, 1964 (1998).
[38]P. G. Bolhuis, D. Chandler, C. Dellago, and P. L. Geissler, "Transition path sampling: Throwing ropes over rough mountain passes, in the dark," Annu. Rev. Phys. Chem. **53**, 291–318 (2002).
[39]T. S. van Erp, D. Moroni, and P. G. Bolhuis, "A novel path sampling method for the calculation of rate constants," J. Chem. Phys. **118**, 7762–7774 (2003).
[40]A. K. Faradjian and R. Elber, "Computing time scales from reaction coordinates by milestoning," J. Chem. Phys. **120**, 10880–10889 (2004).
[41]A. M. A. West, R. Elber, and D. Shalloway, "Extending molecular dynamics time scales with milestoning: Example of complex kinetics in a solvated peptide," J. Chem. Phys. **126**, 145104 (2007).
[42]G. Bussi, F. L. Gervasio, A. Laio, and M. Parrinello, "Free-energy landscape for beta hairpin folding from combined parallel tempering and metadynamics," J. Am. Chem. Soc. **128**, 13435–13441 (2006).
[43]R. J. Allen, D. Frenkel, and P. R. t. Wolde, "Simulating rare events in equilibrium or nonequilibrium stochastic systems," J. Chem. Phys. **124**, 024102 (2006).
[44]E. Vanden-Eijnden, M. Venturoli, G. Ciccotti, and R. Elber, "On the assumptions underlying milestoning," J. Chem. Phys. **129**, 174102 (2008).
[45]K. Kuczera, G. S. Jas, and R. Elber, "Kinetics of helix unfolding: Molecular dynamics simulations with milestoning," J. Phys. Chem. A **113**, 7461–7473 (2009).
[46]B. W. Zhang, D. Jasnow, and D. M. Zuckerman, "The 'weighted ensemble' path sampling method is statistically exact for a broad class of stochastic processes and binning procedures," J. Chem. Phys. **132**, 054107 (2010).
[47]E. Vanden-Eijnden and M. Venturoli, "Markovian milestoning with Voronoi tessellations," J. Chem. Phys. **130**, 194101 (2009).
[48]R. Elber, J. Bello-Rivas, P. Ma, A. Cardenas, and A. Fathizadeh, "Calculating iso-committor surfaces as optimal reaction coordinates with milestoning," Entropy **19**(5), 219 (2017).
[49]J. N. Murrell and K. J. Laidler, "Symmetries of activated complexes," Trans. Faraday Soc. **64**, 371–377 (1968).
[50]D. J. Wales, "Discrete path sampling," Mol. Phys. **100**, 3285–3305 (2002).
[51]D. J. Wales, "Some further applications of discrete path sampling to cluster isomerization," Mol. Phys. **102**, 891–908 (2004).
[52]D. Chakraborty, R. Collepardo-Guevara, and D. J. Wales, "Energy landscapes, folding mechanisms, and kinetics of RNA tetraloop hairpins," J. Am. Chem. Soc. **136**(52), 18052–18061 (2014).
[53]D. Chakraborty and D. J. Wales, "Probing helical transitions in a DNA duplex," Phys. Chem. Chem. Phys. **19**(1), 878–892 (2016).
[54]D. Chakraborty and D. J. Wales, "Energy landscape and pathways for transitions between Watson-Crick and Hoogsteen base pairing in DNA," J. Phys. Chem. Lett. **9**, 229–241 (2018).
[55]I. Yildirim, D. Chakraborty, M. Disney, D. J. Wales, and G. C. Schatz, "Computational investigation of RNA cug repeats responsible for myotonic dystrophy I," J. Chem. Theory Comput. **11**, 4943–4958 (2015).
[56]T. Cragnolini, D. Chakraborty, J. Šponer, P. Derreumaux, S. Pasquali, and D. J. Wales, "Multifunctional energy landscape for a DNA G-quadruplex: An evolved molecular switch," J. Chem. Phys. **147**, 152715 (2017).
[57]J. S. Klimavicz, K. Röder, and D. J. Wales, "Energy landscapes of mini-dumbbell DNA octanucleotides," J. Chem. Theory Comput. **14**, 3870–3876 (2018).
[58]N. B. Leontis and E. Westhof, "Geometric nomenclature and classification of RNA base pairs," RNA **7**, 499–512 (2001).
[59]G. Chen, S. D. Kennedy, J. Qiao, T. R. Krugh, and D. H. Turner, "An alternating sheared AA pair and elements of stability for a single sheared purine-purine pair flanked by sheared GA pairs in RNA," Biochemistry **45**, 6889–6903 (2006).
[60]K. P. Van Nostrand, S. D. Kennedy, D. H. Turner, and D. H. Mathews, "Molecular mechanics investigation of an adenine-adenine non-canonical pair conformational change," J. Chem. Theory Comput. **7**, 3779–3792 (2011).
[61]G. Henkelman, B. P. Uberuaga, and H. Jònsson, "A climbing image nudged elastic band method for finding saddle points and minimum energy paths," J. Chem. Phys. **113**, 9901–9904 (2000).
[62]G. Henkelman and H. Jónsson, "Improved tangent estimate in the nudged elastic band method for finding minimum energy paths and saddle points," J. Chem. Phys. **113**, 9978–9985 (2000).
[63]E. Malolepsza, B. Strodel, M. Khalili, S. Trygubenko, S. N. Fejer, and D. J. Wales, "Symmetrization of the AMBER and CHARMM force fields," J. Comput. Chem. **31**(7), 1402–1409 (2010).
[64]A. Pérez, I. Marchán, D. Svozil, J. Šponer, T. E. Cheatham, C. A. Laughton, and M. Orozco, "Refinement of the amber force field for nucleic acids: Improving the description of $\alpha/\gamma$ conformers," Biophys. J. **92**(11), 3817–3829 (2007).
[65]M. Zgarbová, M. Otyepka, J. Šponer, A. Mládek, P. Banáš, T. E. Cheatham, and P. Jurečka, "Refinement of the Cornell *et al.* nucleic acids force field based on reference quantum chemical calculations of glycosidic torsion profiles," J. Chem. Theory Comput. **7**(9), 2886–2902 (2011).
[66]A. Onufriev, D. Bashford, and D. A. Case, "Exploring protein native states and large-scale conformational changes with a modified generalized born model," Proteins **55**(2), 383–394 (2004).
[67]A. Onufriev, D. Bashford, and D. A. Case, "Modification of the generalized Born model suitable for macromolecules," J. Phys. Chem. B **104**, 3712–3720 (2000).
[68]J. Srinivasan, M. W. Trevathan, P. Beroza, and D. A. Case, "Application of a pairwise generalized Born model to proteins and nucleic acids: Inclusion of salt effects," Theor. Chem. Acc. **101**, 426–434 (1999).
[69]A. W. Gotz, M. J. Williamson, D. Xu, D. Poole, S. Le Grand, and R. C. Walker, "Routine microsecond molecular dynamics simulations with AMBER on GPUs 1. Generalized born," J. Chem. Theory Comput. **8**, 1542–1555 (2012).
[70]D. J. Wales, *Energy Landscapes* (Cambridge University Press, UK, 2003).
[71]D. Liu and J. Nocedal, "On the limited memory method for large scale optimization," Math. Program. **45**, 503–528 (1989).
[72]S. A. Trygubenko and D. J. Wales, "A doubly nudged elastic band method for finding transition states," J. Chem. Phys. **120**, 2082–2094 (2004).
[73]L. J. Munro and D. J. Wales, "Defect migration in crystalline silicon," Phys. Rev. B **59**, 3969–3980 (1999).
[74]Y. Zheng, P. Xiao, and G. Henkelman, "Unification of algorithms for minimum mode optimization," J. Chem. Phys. **140**, 044115 (2014).
[75]D. J. Wales, "OPTIM: A program for geometry optimisation and pathway calculations," http://www-wales.ch.cam.ac.uk/software.html.
[76]D. A. Case, T. A. Darden, T. E. Cheatham, C. L. Simmerling, J. Wang, R. E. Duke, R. Luo, R. C. Walker, W. Zhang, K. M. Merz, B. Roberts, S. Hayik, A. Roitberg, G. Seabra, J. Swails, A. W. Goetz, and I. Kolossváry, AMBER 9, 2006.
[77]D. J. Wales, "PATHSAMPLE: A program for generating connected stationary point databases and extracting global kinetics," http://www-wales.ch.cam.ac.uk/software.html.


Published under license by AIP Publishing

[78]J. M. Carr, S. A. Trygubenko, and D. J. Wales, "Finding pathways between distant local minima," J. Chem. Phys. **122**, 234903 (2005).
[79]B. Strodel, C. S. Whittleston, and D. J. Wales, "Thermodynamics and kinetics of aggregation for the GNNQQNY peptide," J. Am. Chem. Soc. **129**, 16005–16014 (2007).
[80]D. J. Wales, J. M. Carr, M. Khalili, V. K. de Souza, B. Strodel, and C. S. Whittleston, "Pathways and rates for structural transformations of peptides and proteins," in *Proteins: Energy, Heat and Signal Flow, Computation in Chemistry* (CRC Press, 2009), p. 315.
[81]J. M. Carr and D. J. Wales, "Folding pathways and rates for the three-stranded β-sheet peptide Beta3s using discrete path sampling," J. Phys. Chem. B **112**, 8760–8769 (2008).
[82]O. M. Becker and M. Karplus, "The topology of multidimensional potential energy surfaces: Theory and application to peptide structure and kinetics," J. Chem. Phys. **106**, 1495–1517 (1997).
[83]D. J. Wales, M. A. Miller, and T. R. Walsh, "Archetypal energy landscapes," Nature **394**, 758–760 (1998).
[84]S. V. Krivov and M. Karplus, "Free energy disconnectivity graphs: Application to peptide models," J. Chem. Phys. **117**, 10894–10903 (2002).
[85]S. V. Krivov and M. Karplus, "Hidden complexity of free energy surfaces for peptide (protein) folding," Proc. Natl. Acad. Sci. U. S. A. **101**, 14766–14770 (2004).
[86]Y. Chebaro, A. J. Ballard, D. Chakraborty, and D. J. Wales, "Intrinsically disordered energy landscapes," Sci. Rep. **5**, 10386 (2015).
[87]K. Röder and D. J. Wales, "Transforming the energy landscape of a coiled-coil peptide via point mutations," J. Chem. Theory Comput. **13**, 1468–1477 (2017).
[88]J. P. Neirotti, F. Calvo, D. L. Freeman, and J. D. Doll, "Phase changes in 38 atom Lennard Jones clusters. I. A parallel tempering study in the canonical ensemble," J. Chem. Phys. **112**, 10340–10349 (2000).
[89]J. P. K. Doye, M. A. Miller, and D. J. Wales, "The double-funnel energy landscape of the 38-atom Lennard-Jones cluster," J. Chem. Phys. **110**, 6896–6906 (1999).
[90]D. J. Wales, "Calculating rate constants and committor probabilities for transition networks by graph transformation," J. Chem. Phys. **130**, 204111 (2009).
[91]R. S. MacKay and J. D. Robinson, "Aggregation of Markov flows. I. Theory," Philos. Trans. R. Soc., A **376**(2118), 20170232 (2018).
[92]I. Yildirim, S. D. Kennedy, H. A. Stern, J. M. Hart, R. Kierzek, and D. H. Turner, "Revision of AMBER torsional parameters for RNA improves free energy predictions for tetramer duplexes with GC and iGiC base pairs," J. Chem. Theory Comput. **8**, 172–181 (2012).
[93]A. H. Aytenfisu, A. Spasic, A. Grossfield, H. A. Stern, and D. H. Turner, "Revised RNA dihedral parameters for the AMBER force field improve RNA molecular dynamics," J. Chem. Theory Comput. **13**, 900–915 (2017).
[94]A. Gil-Ley, S. Bottaro, and G. Bussi, "Empirical corrections to the AMBER RNA force field with target metadynamics," J. Chem. Theory Comput. **12**, 2790–2798 (2016).
[95]A. Cesari, A. Gil-ley, and G. Bussi, "Combining simulations and solution experiments as a paradigm for RNA force field refinement," J. Chem. Theory Comput. **12**, 6192–6200 (2016).
[96]D. J. Wales and I. Yildirim, "Improving computational predictions of single-stranded RNA tetramers with revised $\alpha/\gamma$ torsional parameters for the AMBER force field," J. Phys. Chem. B **121**, 2989–2999 (2017).
[97]D. Tan, S. Piana, R. M. Dirks, and D. E. Shaw, "RNA force field with accuracy comparable to state-of-the-art protein force fields," Proc. Natl. Acad. Sci. U. S. A. **115**, E1346–E1355 (2018).
[98]J. Šponer, G. Bussi, M. Krepl, P. Baná Š, S. Bottaro, R. A. Cunha, A. Gil-Ley, G. Pinamonti, S. Poblete, P. Jurečka, N. G. Walter, and M. Otyepka, "RNA structural dynamics as captured by molecular simulations: A comprehensive overview," Chem. Rev. **118**(8), 4177–4338 (2018).
[99]G. M. Giambasu, D. M. York, and D. A. Case, "Structural fidelity and NMR relaxation analysis in a prototype RNA hairpin," RNA **21**, 963–974 (2015).
[100]N. A. Denesyuk and D. Thirumalai, "How do metal ions direct ribozyme folding?," Nat. Chem. **7**, 793–801 (2015).
[101]M. R. Hoare and J. J. McInnes, "Statistical mechanics and morphology of very small atomic clusters," Faraday Discuss. Chem. Soc. **61**, 12–24 (1976).
[102]M. R. Hoare, *Advances in Chemical Physics* (John Wiley & Sons, USA, 1979), Vol. 40, pp. 49–129.
[103]J. M. Carr and D. J. Wales, "The energy landscape as a computational tool," in *Latest Advances in Atomic Cluster Collisions: Structure and Dynamics from the Nuclear to the Biological Scale*, edited by J.-P. Connerade and A. Solov'yov (Imperial College Press, London, 2008), pp. 321–330.
[104]V. M. Jiménez and A. Marzal, "Computing the *k* shortest paths: A new algorithm and an experimental comparison," in *Algorithm Engineering: 3rd International Workshop, WAE'99, London, UK, July 1999*, edited by J. S. Vitter and C. D. Zaroliagis (Springer Berlin/Heidelberg, 1999), Vol. 1668, pp. 15–29.
[105]J. M. Carr and D. J. Wales, "Refined kinetic transition networks for the GB1 hairpin peptide," Phys. Chem. Chem. Phys. **11**, 3341–3354 (2009).
[106]J. D. Stevenson and D. J. Wales, "Analysing kinetic transition networks for rare events," J. Chem. Phys. **141**, 041104 (2014).
[107]D. J. Wales and P. Salamon, "Observation time scale, free-energy landscapes, and molecular symmetry," Proc. Natl. Acad. Sci. U. S. A. **111**, 617–622 (2014).


Published under license by AIP Publishing